

# Transport and the Order Parameter of Superconducting $\text{UPt}_3$

W. C. Wu<sup>1</sup> and R. Joynt<sup>2</sup>

<sup>1</sup>*Department of Physics, National Taiwan Normal University, Taipei 11650, Taiwan*

<sup>2</sup>*Department of Physics, University of Wisconsin-Madison, Madison, WI 53706*

(Dated: November 10, 2018)

We calculate the ultrasonic absorption and the thermal conductivity in the superconducting state of  $\text{UPt}_3$  as functions of temperature and direction of propagation and polarization. Two leading candidates for the superconducting order parameter are considered: the  $E_{1g}$  and  $E_{2u}$  representations. Both can fit the data except for the ultrasonic absorption in the  $A$  phase. To do that, it is necessary to suppose that the system has only a single domain, and that must be chosen as the most favorable one. However, the  $E_{2u}$  theory requires fine-tuning of parameters to fit the low temperature thermal conductivity. Thus, transport data favor the  $E_{1g}$  theory. Measurements of the thermal conductivity as a function of pressure at low temperature could help to further distinguish the two theories.

PACS numbers: 74.70.Tx, 74.20.Rp, 74.25.Ld

## I. INTRODUCTION

$\text{UPt}_3$  continues to pose a fundamental challenge to solid-state physics. It becomes superconducting at about  $T_{c+} = 0.5K$ , entering the  $A$  phase, and has a second transition at about  $T_{c-} = 0.44K$  entering the  $B$  phase. Its unusual phase diagram and thermodynamics show that it is unconventional. The precise nature of its superconducting order parameter remains elusive, however.

From the purely theoretical point of view, order parameters (OPs) that transform according to a single representation of the  $D_{6h}$  group and that take into account spin-orbit coupling are the most desirable. This includes the  $E_{1g}$  [1] and  $E_{2u}$  [2] theories. Because of the perception that these theories may not give sufficient phenomenological flexibility, other pictures have been constructed. One of these is the mixed-representation (*e.g.*,  $A$ - $B$ ) [3] picture. This suffers from the problem of fine tuning, since the coupling constants of the two representations must be nearly identical to account for the nearness of  $T_{c+}$  and  $T_{c-}$ . Another picture is the extended-symmetry-group spin triplet theory [4]. However, this requires zero spin-orbit coupling in an  $f$ -electron system, an artificial assumption.

From the point of view of comparison to experiment, the most stringent constraints on theory come from detailed measurements of the thermal conductivity  $\kappa$  [5] and the ultrasonic attenuation  $\alpha$  [6]. Because of the directional information inherent in these probes, they offer the best chance to distinguish between order parameters that may have only relatively subtle differences [7]. This expectation is reinforced by the fact that the ultrasonic attenuation has been measured in the  $A$  phase, the most anisotropic of the zero-field phases. Previous calculations have indicated that the mixed representation and extended symmetry group scenarios are probably inconsistent with these measurements [8]. Accordingly we focus in this paper on the  $E_{1g}$  and  $E_{2u}$  theories. Our aim is to compare theory and experiment for  $\kappa$  and  $\alpha$  in a quantitative fashion. In so doing, we can also investigate whether fine-tuning is required in either of these

pictures.

In the next section, we give the details of the calculation. The following section compares the fits for the two models. The final section discusses how the models can be distinguished on the basis of pressure experiments and gives a brief summary.

## II. CALCULATION METHOD

### A. Bands

The Fermi surface of  $\text{UPt}_3$  is highly complex. There are five or six sheets, some having a very complicated shape. However, the effective masses of the sheets have been very accurately determined for most directions by de Haas-van Alphen experiments [9]. These measurements show that the  $\Gamma_3$  sheet contains about 80% of the density of states at the Fermi energy  $\epsilon_F$ . This sheet is centered on the  $\Gamma$  point. We approximate it as an ellipsoid with a dispersion relation:

$$\epsilon_{\mathbf{k}} = \frac{\hbar^2}{2} \left( \frac{k_x^2}{m_x} + \frac{k_y^2}{m_y} + \frac{k_z^2}{m_z} \right) - \epsilon_F, \quad (1)$$

with  $m_z = 43.2m_e$  and  $m_x = m_y = 17.4m_e$ . The small “eggs” of the  $\Gamma_3$  band at the zone boundary are ignored. We have investigated the effect of including other bands and find that the contributions are small. The anisotropic mass in the  $\Gamma_3$  band is very important, however. The results are quite different for an isotropic Fermi surface.

### B. Order Parameters

The central part of the  $\Gamma_3$  band does not cross the Brillouin zone boundary. This means that nodes coming from the fact that gap functions should be invariant under translation by a reciprocal lattice vector do not need

to be considered. In this case, to good accuracy, one can use polynomial functions to describe the gap functions.

Standard calculations for the  $E_{1g}$  model use a singlet gap function

$$\Delta(\mathbf{k}) = \Delta_0(T) [k_z k_x + i \delta(T) k_z k_y], \quad (2)$$

while for the  $E_{2u}$  model conventional calculations use the triplet gap function

$$\mathbf{d}(\mathbf{k}) = \Delta_0(T) \hat{z} [k_z(k_x^2 - k_y^2) + 2i\delta(T)k_z k_x k_y], \quad (3)$$

where  $k_\mu$  is the  $\mu$ -component of  $\mathbf{k}$  vector on the Fermi surface and  $\hat{z}$  is the direction of the vector  $\mathbf{d}(\mathbf{k})$  in pseudospin space. Both models involve the idea that the  $A$  phase involves only a single OP component: in the  $A$  phase,  $\delta(T) = 0$ . Accordingly,  $\delta(T)$  is a temperature-dependent function that begins to grow continuously at the  $A$ - $B$  phase boundary.

A crucial point in the theoretical treatment, however, is that the expressions in Eqs. (2) and (3) are *not* the complete OPs for these representations. Yip and Garg [10] have shown that the complete gap functions for these phases are linear combinations of two pairs of functions for  $E_{1g}$  rather than the single pair  $(k_z k_x, k_z k_y)$  shown in Eq. (2). For  $E_{2u}$ , the gap function is a linear combination of six pairs rather than the single pair  $(\hat{z}k_z(k_x^2 - k_y^2), \hat{z}k_z k_x k_y)$ . Writing the complete gap functions in the form appropriate for use in both the  $A$  and  $B$  phases, we have the formulas

$$\Delta(\mathbf{k}) = \Delta_0(T) \sum_{n=1}^2 g^{(n)} [f_x^{(n)}(\mathbf{k}) + i\delta(T)f_y^{(n)}(\mathbf{k})] \quad (4)$$

for  $E_{1g}$  and

$$\mathbf{d}(\mathbf{k}) = \Delta_0(T) \sum_{n=1}^6 u^{(n)} [\mathbf{f}_x^{(n)}(\mathbf{k}) + i\delta(T)\mathbf{f}_y^{(n)}(\mathbf{k})] \quad (5)$$

for  $E_{2u}$ . The functions  $f(\mathbf{k})$  and  $\mathbf{f}(\mathbf{k})$  are defined in Tables I and II, adapted from Ref. [10]. In the  $E_{1g}$  representation, the gap function is a linear combination of the two functions in the first column of Table I. In the  $B$  phase, the functions in the second column also come in, with a relative phase of  $i$ , as shown in Eq. (4). In the  $E_{2u}$  representation, the gap function is a linear combination of the six functions in the first column of Table II. In the  $B$  phase, the functions in the second column also come in, with a relative phase of  $i$ , as shown in Eq. (5). Note that

the resulting gap function can be multiplied by another completely symmetric ( $A_{1g}$ ) function without changing its symmetry. Nearly all calculations for  $E_{1g}$  have set  $g^{(2)} = 0$ , while nearly all calculations for  $E_{2u}$  have set  $u^{(1)} = u^{(3)} = u^{(4)} = u^{(5)} = u^{(6)} = 0$ . (For an exception see Ref. [11]).

It is very important to understand what this special choice of  $g^{(n)}$  or  $u^{(n)}$  implies. There are two levels of

TABLE I: Basis functions for the  $E_{1g}$  representation.

	$f_x^{(n)}(\mathbf{k})$	$f_y^{(n)}(\mathbf{k})$
$n = 1$	$k_x k_z$	$k_y k_z$
$n = 2$	$(k_x^5 - 10k_x^3 k_y^2 + 5k_x k_y^4)k_z$	$(k_y^5 - 10k_y^3 k_x^2 + 5k_y k_x^4)k_z$

doing phenomenology for the OP. One is choosing a representation and working out the consequences. In this case the coefficients  $g^{(n)}$  and  $u^{(n)}$  must be treated as parameters. They are *continuous* functions of all the many parameters that are in the microscopic Hamiltonian, as well as external variables such as pressure. Thus choosing a representation means choosing a *set* of Hamiltonians of finite measure, i.e., to selecting an alternative that has a finite *a priori* probability. The other (more commonly used) level of phenomenology is to choose a specific basis function from Table I or Table II and work out the consequences. This means setting all but one of the  $g^{(n)}$  or  $u^{(n)}$  equal to zero. It also means choosing a set of Hamiltonians of zero measure, which has zero *a priori* probability. In other words, choosing a specific basis function amounts to fine tuning. None of the  $g^{(n)}$  or  $u^{(n)}$  can vanish by symmetry, since all symmetries of the system have already been taken into account in the group-theoretical decomposition.

This does not necessarily invalidate previous work that has been done with a specific choice of basis function. If the comparison to experimental data is not very sensitive to variations in  $g^{(n)}$  or  $u^{(n)}$ , then the fine tuning may be abandoned without harming agreement of theory and observation. A key goal of this paper is to investigate this sensitivity for the  $E_{1g}$  and  $E_{2u}$  theories.

### C. Transport Coefficients

Ultrasonic attenuation experiments in UPT<sub>3</sub> have been done in the hydrodynamic regime where the sound frequency  $\omega$  satisfies  $\omega < 1/\tau_s$ , with  $\tau_s$  the electronic relaxation time. The appropriate formula for sound propagation along the direction  $\hat{q}$  with polarization  $\hat{\varepsilon} \perp \hat{q}$  is:

$$\alpha_{\hat{q}\hat{\varepsilon}}(T) \propto \int_0^\infty d\omega \left[ -\frac{\partial F(\omega)}{\partial \omega} \right] \tau_s(\omega, T) \left\langle \text{Re} \left( \frac{\sqrt{\omega^2 - |\Delta_{\mathbf{k}}|^2}}{\omega} (\hat{q} \cdot \hat{\mathbf{k}})^2 (\hat{\varepsilon} \cdot \hat{\mathbf{k}})^2 \right) \right\rangle. \quad (6)$$

TABLE II: Basis functions for the  $E_{2u}$  representation.

	$\mathbf{f}_x^{(n)}(\mathbf{k})$	$\mathbf{f}_y^{(n)}(\mathbf{k})$
$n = 1$	$k_x \hat{x} - k_y \hat{y}$	$k_y \hat{x} + k_x \hat{y}$
$n = 2$	$(k_x^2 - k_y^2)k_z \hat{z}$	$2k_x k_y k_z \hat{z}$
$n = 3$	$(k_x^3 - 3k_x k_y^2) \hat{x} - (k_y^3 - 3k_y k_x^2) \hat{y}$	$(k_x^3 - 3k_x k_y^2) \hat{y} + (k_y^3 - 3k_y k_x^2) \hat{x}$
$n = 4$	$(k_x^3 - 3k_x k_y^2) \hat{x} + (k_y^3 - 3k_y k_x^2) \hat{y}$	$(k_x^3 - 3k_x k_y^2) \hat{y} - (k_y^3 - 3k_y k_x^2) \hat{x}$
$n = 5$	$(k_x^4 - 6k_x^2 k_y^2 + k_y^4)k_z \hat{z}$	$(4k_x^3 k_y - 4k_x k_y^3)k_z \hat{z}$
$n = 6$	$(k_x^5 - 10k_x^3 k_y^2 + 5k_x k_y^4) \hat{x} + (k_y^5 - 10k_y^3 k_x^2 + 5k_y k_x^4) \hat{y}$	$(k_x^5 - 10k_x^3 k_y^2 + 5k_x k_y^4) \hat{y} - (k_y^5 - 10k_y^3 k_x^2 + 5k_y k_x^4) \hat{x}$

Here  $F$  is the Fermi function and the angle brackets indicate a Fermi surface average.  $|\Delta_{\mathbf{k}}|^2 \rightarrow |\mathbf{d}_{\mathbf{k}}|^2$  in the triplet case. The thermal conductivity in the  $i$ th direction when

a temperature gradient is imposed along the  $i$ th direction is computed using:

$$\kappa_{ii}(T) \propto \frac{1}{T} \int_0^\infty d\omega \omega^2 \left[ -\frac{\partial F(\omega)}{\partial \omega} \right] \tau_s(\omega, T) \left\langle \text{Re} \left( \frac{\sqrt{\omega^2 - |\Delta_{\mathbf{k}}|^2}}{\omega} (\hat{i} \cdot \hat{\mathbf{k}})^2 \right) \right\rangle. \quad (7)$$

The prefactors are fitted to the values of  $\alpha_{\hat{\mathbf{q}}\hat{\boldsymbol{\varepsilon}}}$  and  $\kappa_{ii}$  at  $T_{c+}$ .

Our approach does not calculate the density of states self-consistently. This means that it is not very accurate at low temperatures,  $T < 0.2T_{c+}$ , but in this paper we are chiefly concerned with the behavior closer to  $T_{c+}$ .

The temperature dependence of  $\Delta_0(T)$  is not accurately known. However, one may deduce the power law at low temperature from the pattern of nodes, while near  $T_c$  we can use Ginzburg-Landau theory for the same purpose. For computational convenience, we take  $\delta(T) = [1 - (T/T_{c-})^6]^{1/2}$  and  $\Delta_0(T) = \Delta_0(T = 0) [1 - (T/T_{c+})^x]^{1/2}$ .  $x = 2$  and  $x = 3$  for point and line nodes, respectively. We have verified that these functions are close to the Ginzburg-Landau result near  $T_{c+}$  and they have the appropriate behavior at low temperature as well. In addition, this leads to a fit for the temperature dependence with only the single parameter  $\Delta_0(T = 0)$ . Finally, we follow *Graf et al.* [8] in taking the empirical form for the relaxation time:  $\tau_s \simeq 0.01\pi T_{c+}(1 + T^2/T_{c+}^2)$ .

#### D. Domains

In the A phase there is an additional complication.  $\delta(T) = 0$  so that, as stated above, only the  $f_x(\mathbf{k})$  (or  $\mathbf{f}_x(\mathbf{k})$ ) functions are used. However, the theory requires that the superconducting OP is oriented by its coupling to the staggered antiferromagnetic moment  $\mathbf{M}_S$ . There are three domains allowed by symmetry for  $\mathbf{M}_S$ , and neutron scattering experiments show that they are equally populated. The pattern of nodes rotates by  $\pi/6$  around the  $c$ -axis every time the wave passes through a domain

wall. The gap function becomes, for example,  $f_x(\mathcal{R}\mathbf{k})$  where  $\mathcal{R}\mathbf{k}$  is the rotated vector. We shall take a coordinate system which is fixed in the laboratory: the propagation vector or polarization vectors refer to this frame.

The observed  $\alpha$  must result from an average over domains. In such a situation, response functions are usually calculated by effective medium theory, which may take various forms, depending on the approximations made [12]. However, the present case is simplified by the fact that  $\alpha$  is the relatively small imaginary part of a large complex quantity, the sound propagation vector. For such a perturbative quantity, all averaging methods lead to the result that the observed global  $\alpha$  should be the mean of the three local values.

### III. RESULTS

#### A. Best fits

We begin the comparison of theory and experiment in this subsection by adjusting all parameters in Eqs. (4) and (5) to their optimum values for both representations, varying the mass anisotropy  $m_z/m_x$  and choosing the most favorable domain of the A phase. Fairly impressive fits of data to experiment for both theories may be obtained in this way.

The best fits for  $E_{1g}$  and  $E_{2u}$  models for the ultrasound and the thermal conductivity are plotted against the data in Fig. 1. The curves for  $\kappa$  provide reasonable fits over the whole range of temperature. In particular, the overall *anisotropy* is well fit. Some discrepancies may be noted at sufficiently low temperature. The fits for  $\alpha$  are also

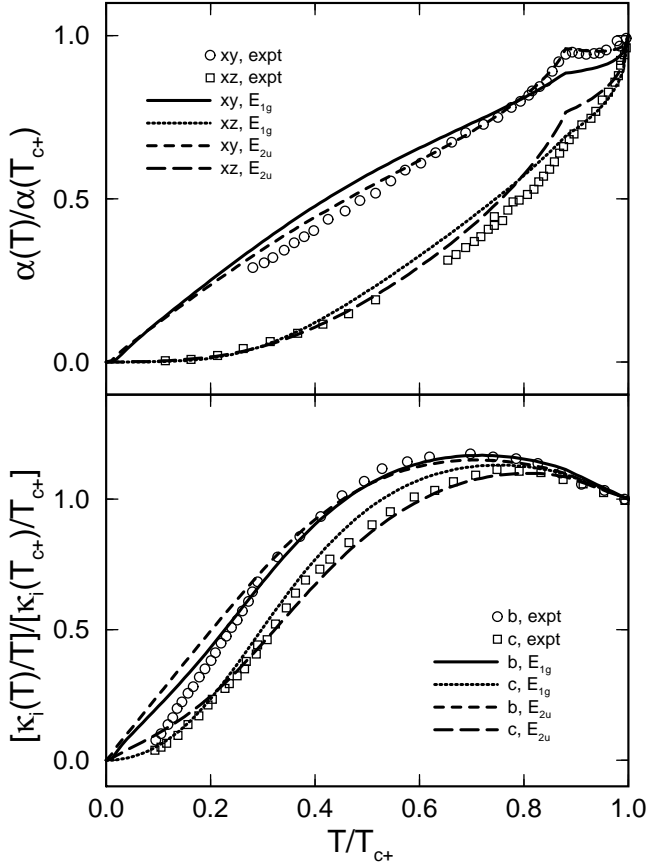


FIG. 1: Best fits of  $E_{1g}$  and  $E_{2u}$  models against the data [15, 16] for both transverse sound attenuation (top frame) and thermal conductivity (bottom frame). The fitting parameters are given in the text.

reasonable except that some minor discrepancies may be noted near  $T_c$  in the  $A$  phase. The best-fit parameters for  $E_{1g}$  are:  $\Delta(0) = 3T_{c+}$ ,  $x = 2$ , and  $g^{(1)} = 1.0$  and  $g^{(2)} = 0.2$ , while the best-fit parameters for  $E_{2u}$  are:  $\Delta(0) = 4.5T_{c+}$ ,  $x = 2$ , and all the coefficients  $u^{(i)}$  vanish except  $u^{(2)} = 1.0$ .

There exists a major difference between the best fits of  $E_{1g}$  and  $E_{2u}$  models when anisotropic masses are considered. For  $E_{1g}$ , the anisotropic mass ratio is fixed as  $m_z/m_x = m_z/m_y = 2.5$ . This agrees with the measured value [9] for the dominant  $\Gamma_3$  band. For  $E_{2u}$ , in contrast, the best fits are acquired at  $m_z/m_x = m_z/m_y = 0.33$ , in very poor agreement with the measured value.

### B. Anisotropic mass

In order to give some idea of the sensitivity of the fits to the anisotropic mass ratio, we calculate  $\alpha$  and  $\kappa$  for  $E_{2u}$  model using the same best-fit parameters except for the anisotropic mass ratio  $m_z/m_x$ . As seen in Fig. 2, as the ratio is increased from 0.33 to its physical value of 2.5, the polarization anisotropy in  $\alpha$  decreases sharply, while

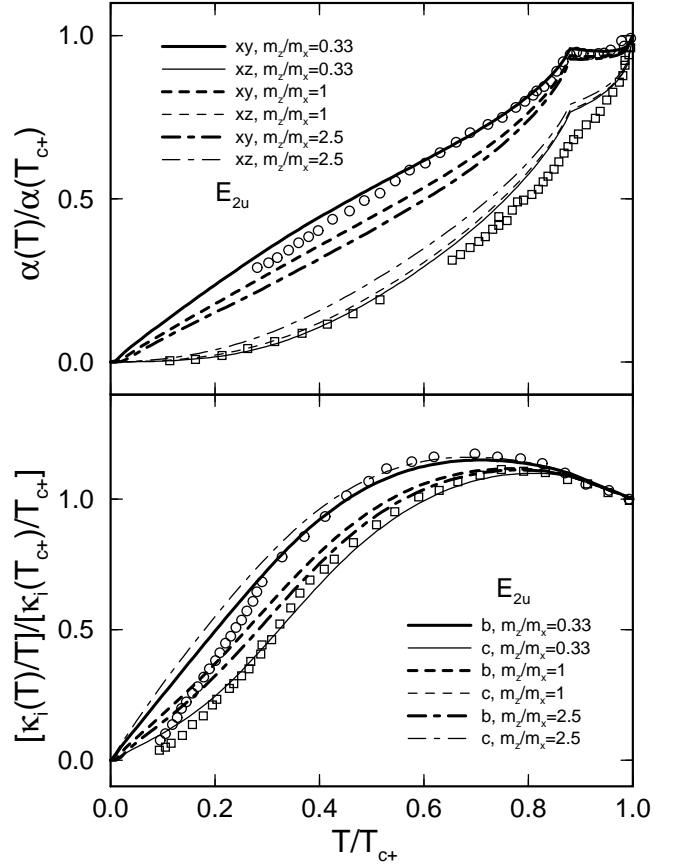


FIG. 2: The figure shows the sensitivity of the fits to the change of the anisotropic mass ratio. In the bottom frame, the two curves ( $b$  and  $c$ ) are indistinguishable for the  $m_z/m_x = 1$  case.

the anisotropy in  $\kappa$  actually reverses. This indicates that the fit for the  $E_{2u}$  model is somewhat questionable.

Our fitting procedure differs from that of Graf *et al.* [8, 13]. These authors used revised order parameters

$$\Delta(\mathbf{k}) = \Delta_0(T) [k_z k_x + i \delta(T) k_z k_y] (1 + a_2 k_z^2 + a_4 k_z^4) \quad (8)$$

for  $E_{1g}$  and

$$\mathbf{d}(\mathbf{k}) = \Delta_0(T) \hat{z} [k_z (k_x^2 - k_y^2) + 2i \delta(T) k_z k_x k_y] (1 + a_2 k_z^2 + a_4 k_z^4) \quad (9)$$

for  $E_{2u}$ , where the coefficients  $a_2$  and  $a_4$  are adjustable fitting parameters. Since the additional factor is completely symmetric, this does not change the representation. As opposed to using the standard basis functions ( $a_2 = a_4 = 0$ ), it is evident that large  $a_2$  and  $a_4$  will correspond to more electronic excitations around the line of nodes at  $k_z = 0$ . This in turn will enhance the in-plane thermal conductivity and sound attenuation relative to the out-of-plane ones. Roughly speaking, the larger  $a_2$  or

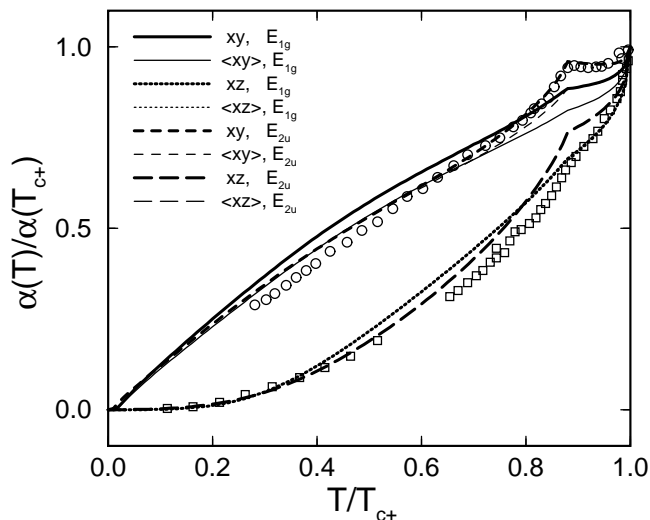


FIG. 3: The best fits of ultrasound attenuation data taking into account three equal-populated domain average. The best fits for one single domain (see also Fig. 1) are included for comparison. The curves for  $xz$  and  $\langle xz \rangle$  are indistinguishable.

$a_4$  case for the revised model is physically analogous to having  $m_x, m_y > m_z$  (and hence larger in-plane density of states) in the standard model. This change in the gap function amounts to multiplying the relative contribution of the in-plane excitations by a factor of 12 relative to what one would expect from the measured ratio of effective masses.

### C. Domain-averaged fits

In order to fit the data in the  $A$  phase, it is necessary to choose the most favorable domain. This was also found by Graf *et al.* [8]. As mentioned above, this is not consistent with the assumptions of the theory. The idea that the order parameter is oriented by  $\mathbf{M}_S$  is a central assumption for both pictures, since it accounts for the fact that  $H_{c2}$  is isotropic in the basal plane. Thus domain averaging is not optional: it is necessary for the consistency of the theory.

If the absorption is properly averaged over all three domains, then we obtain the best fit for the two theories shown in Fig. 3. In the  $A$  phase, the fits are substantially worse than those one gets by choosing the best domain, as was done for Fig. 1 and in Ref. [8].

The reason for the difference in the quality of fit in the  $A$  phase is mainly due to the node patterns. In the  $B$  phase, for both  $E_{1g}$  and  $E_{2u}$  models, there are lines of nodes along the equator and point nodes at the poles of the Fermi surface. In this phase, the nodal pattern is symmetric about the  $c$ -axis and thus the real nodal structures are virtually the same in the three different domains. In the  $A$  phase, in contrast, the two point nodes at the pole have connected to form line nodes in the  $k_x = 0$

plane for  $E_{1g}$  and the  $k_x = \pm k_y$  planes for  $E_{2u}$  model (in the domain defined by the basis functions of Tables I and II). In this case, the nodal structure is asymmetric about the  $c$ -axis. Depending on the orientation of the node pattern relative to the direction of polarization/propagation, the three domains contribute differently. As a matter of fact, as compared to an isotropic state, transverse sound with  $\hat{\mathbf{q}} \parallel \hat{x}$  and  $\hat{\epsilon} \parallel \hat{y}$  (denoted as  $xy$ ) will cause fewer excitations in the  $\pi/6$  or  $\pi/3$  rotated domains. It is this that causes the  $\langle xy \rangle$  (the angle brackets indicate a three equal-populated domains average) attenuation to drop significantly in the  $A$  phase relative to the  $xy$  attenuation. In contrast, the best fits for the  $xz$  and  $\langle xz \rangle$  attenuations are almost indistinguishable. These considerations apply equally to the  $E_{1g}$  and  $E_{2u}$  models.

### D. Fine tuning

An important criterion for the acceptance of a theory is its robustness. If small changes in the parameters would spoil the agreement with the data, the theory is not acceptable since it lacks explanatory power. Accordingly, we investigate the sensitivity of the OP's transport characteristics to changes in its shape. We shall focus on the  $B$  phase for reasons that will become clear below.

For  $E_{1g}$ , varying the shape is relatively straightforward. There are only two parameters  $g^{(1)}$  and  $g^{(2)}$ . In the  $B$  phase with  $g^{(2)} = 0$  there are lines of nodes along the equator and point nodes at the poles. Changing the ratio of  $g^{(1)}$  and  $g^{(2)}$  does not affect this nodal pattern. A larger value of  $g^{(2)}$  merely gives additional modulation to the order parameter in the azimuthal direction. We show some representative curves for  $\kappa_c/\kappa_b$  for different values of the ratio in Fig. 4(a). There is very little change in the goodness of fit as the ratio is varied. Defining a chi-square parameter for the fits as a function of  $g^{(2)}/g^{(1)}$ , we see from its approximate constancy that the  $E_{1g}$  theory is robust for this particular quantity.

The  $E_{2u}$  order parameter behaves very differently. For starters, the shape space  $u^{(1)}, \dots, u^{(6)}$  is six-dimensional. This precludes an extensive search. However, mapping of a two-dimensional subspace will suffice to make the point about parameter sensitivity. The main difference between  $E_{2u}$  and  $E_{1g}$  is clear from the nodal pattern. Taking into account  $u^{(1)}$  in addition to the usual  $u^{(2)}$ , when  $u^{(1)} = 0$  there is a line of nodes at the equator and point nodes at the poles in the  $B$  phase. When  $u^{(1)}$  is finite, however, the line of nodes disappears. This is a consequence of Blount's theorem [14], which states that triplet states in a spin-orbit coupled system do not have lines of nodes. In Fig. 4(b), we show some representative curves for  $\kappa_c/\kappa_b$  for different values of the ratio  $u^{(1)}/u^{(2)}$ . The curves are very sensitive to the ratio, in particular at low temperatures. The chi-square parameter varies rapidly as a function of  $u^{(1)}/u^{(2)}$ . We conclude that the  $E_{2u}$  theory is not robust. Its virtues in describing the data arise from a fine-tuning of the parameters.

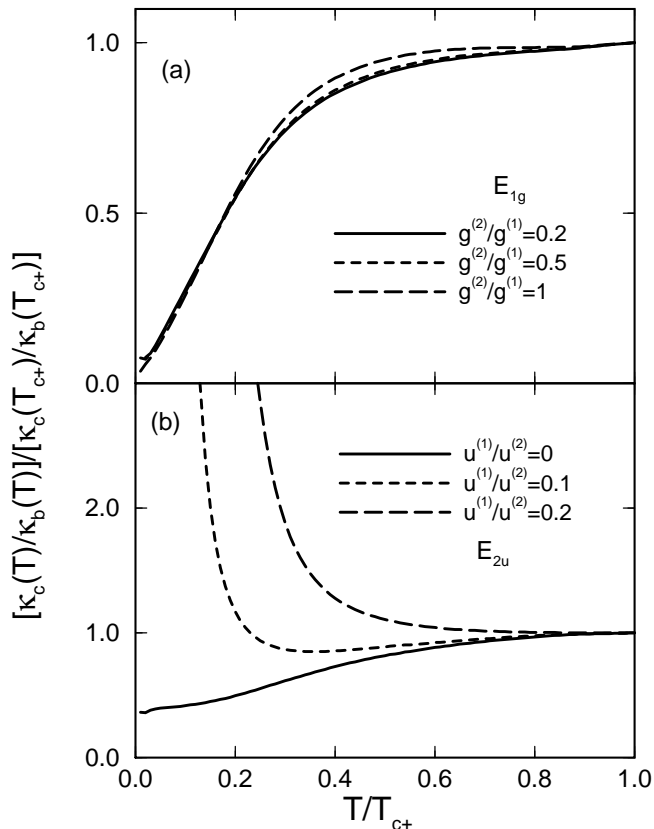


FIG. 4: (a) The ratio of  $\kappa_c/\kappa_b$  for different ratios of  $g^{(2)}/g^{(1)}$  for the  $E_{1g}$  model. (b) The ratio of  $\kappa_c/\kappa_b$  for different ratios of  $u^{(1)}/u^{(2)}$  for the  $E_{2u}$  model.

#### IV. CONCLUSION

Order parameters belonging to the two-dimensional representations  $E_{1g}$  and  $E_{2u}$  remain as the main candidates for the superconducting state of  $\text{UPt}_3$ . A difficulty that remains for both these theories is the explanation of the ultrasonic absorption in the  $A$  phase. The theories require that the observed absorption be the result of an average over three domains in which the order parameter has three orientations. This averaging is deleterious to the agreement between theory and experiment.

This may indicate that there is something wrong with the idea that the magnetization orients the superconductivity, or it may indicate that there is an additional scattering mechanism, such as scattering from domain walls, which partially cancels the drop in absorption due to gap formation.

The  $E_{2u}$  theory has an additional severe problem at low temperatures. A line of nodes at the equator of the Fermi surface is required in order to give agreement with experiment for the thermal conductivity. In the six-dimensional parameter space of this theory, this occurs only in a two-dimensional subspace. The theory therefore requires fine-tuning to explain the data: all the parameters in the microscopic interaction must conspire to give the desired result. It has been suggested that strong spin-orbit coupling can lock the  $\mathbf{d}$ -vector along the  $z$ -direction. However,  $\mathbf{d}$  does not have the interpretation of zero spin projection, as it does in  $^3\text{He}$ . Taking into account the spin-orbit coupling reduces the order parameter space to six dimensions for triplet  $E_2$ , not one or two.

Since the shape parameters  $u^{(n)}$  depend on all the details of the microscopic Hamiltonian, the low temperature power laws that depend on having a line of nodes are unstable. By contrast, the line of nodes at the equator in the  $E_{1g}$  theory is forced by symmetry. Application of *pressure*, for example would lift these nodes in an  $E_{2u}$  gap. The pressure scale that governs superconducting phenomena may be estimated as  $T_{c+}(dT_{c+}/dP)^{-1} \sim 1\text{kbar}$ . One would expect very strong pressure dependence of the thermal conductivity on this scale at low temperatures for  $E_{2u}$  but not for  $E_{1g}$ . This could serve to further distinguish the two theories.

The data presently give preference to the  $E_{1g}$  theory since it does not require fine tuning to explain the data. The discrepancy of theory and experiment for ultrasonic absorption in the  $A$  phase has not been resolved, and may require new ideas.

#### Acknowledgments

Financial support from NSC of Taiwan (Grant No. 90-2112-M-003-018) and the NSF under the Materials Theory program, Grant No. DMR-0081039 is acknowledged.

- 
- [1] K. Park and R. Joynt, Phys. Rev. B **53**, 12346 (1996).
  - [2] J.A. Sauls, Adv. Phys. **43**, 113 (1994).
  - [3] A. Garg and D.-C. Chen, Phys. Rev. B **49**, 479 (1994).
  - [4] K. Machida and M. Ozaki, J. Phys. Soc. Japan **58**, 2244 (1989).
  - [5] H. Suderow, J.P. Brison, A. Huxley, and J. Flouquet, Phys. Rev. Lett. **80**, 165 (1998).
  - [6] B.S. Shivaram, T.F. Rosenbaum, and D. G. Hinks, Phys. Rev. Lett. **57**, 1259 (1986); P. Thalmeier, B. Wolf, D. Weber, R. Blick, G. Bruls, and B. Lüthi, J. Magn. Magn. Mater. **108**, 109 (1992).
  - [7] L. Coffey, T.M. Rice, and K. Ueda, J. Phys. C: Solid State Phys. **18**, L813 (1985); J. Moreno and P. Coleman, Phys. Rev. B **53**, R2995(1996).
  - [8] M. J. Graf, S.-K. Yip, and J. A. Sauls, Phys. Rev. B **62**, 14393 (2000).
  - [9] M.R. Norman, R.C. Albers, A.M. Boring, and N.E. Christensen, Sol. St. Comm. **68**, 245 (1988); L. Taillefer and G.G. Lonzarich, Phys. Rev. Lett. **60**, 1570 (1988).
  - [10] S.-K. Yip and A. Garg, Phys. Rev. B **48**, 3304 (1993).
  - [11] M.R. Norman and P.J. Hirschfeld, Phys. Rev. B **53**, 5706 (1996).

- [12] T. C. Choy, *Effective Medium Theory : Principles and Applications* (Oxford University Press, Oxford, 1999).
- [13] M. J. Graf, S.-K. Yip, and J. A. Sauls, *J. Low Temp. Phys.* **102**, 367 (1996).
- [14] E. Blount, *Phys. Rev. B* **32**, 2935 (1985).
- [15] B. Ellman, L. Taillefer, and M. Poirier, *Phys. Rev. B* **54**, 9043 (1996).
- [16] B. Lussier, B. Ellman, and L. Taillefer, *Phys. Rev. B* **53**, 5145 (1996).